

FULL PAPER

Open Access



XYtracker: a new approach to estimate fault rupture extent in real time for large earthquakes

Ying Xiao^{1,2} and Masumi Yamada^{3*}

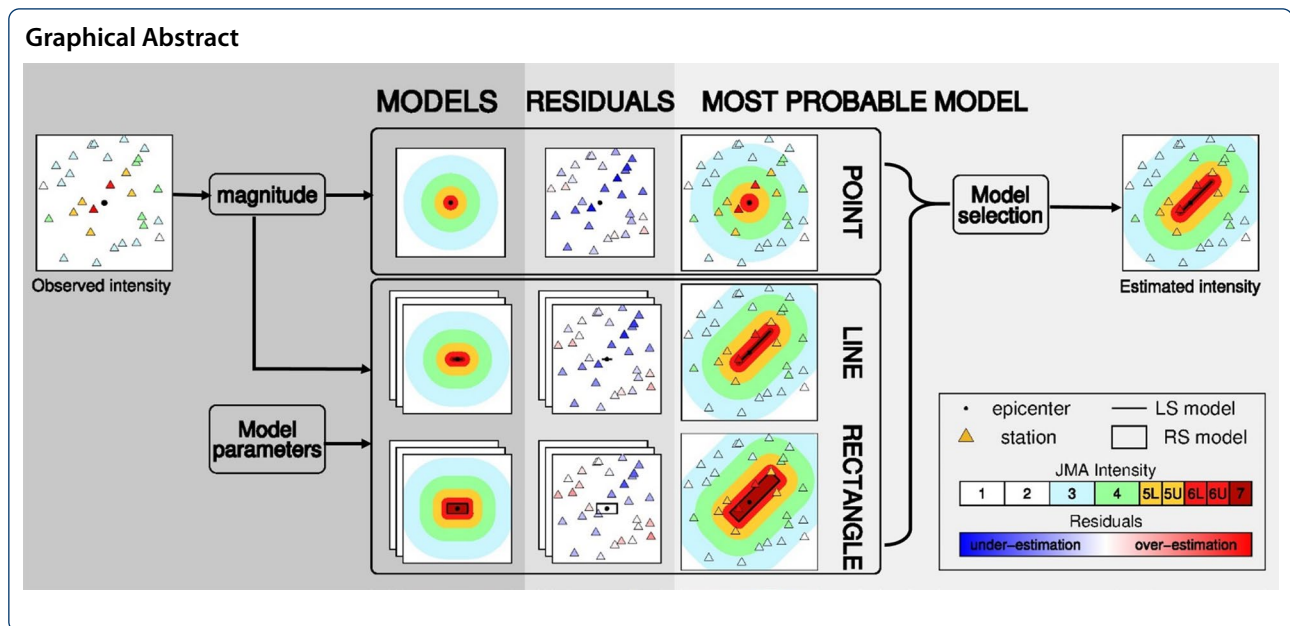
Abstract

We present a methodology for estimating fault geometry and utilizing the distance to the fault for the shaking estimation to improve the accuracy of real-time shaking estimates for large earthquakes. Most of the earthquake early warning system currently estimates the seismic intensity with the ground-motion prediction equations (GMPE) as a function of the hypocenter distance. However, using the fault distance computed from a finite source model can improve the accuracy of the shaking intensity estimation for large earthquakes. This study proposes a novel methodology, XYtracker, to estimate the surface projection of the fault extent and real-time seismic intensity. For large earthquakes, high-frequency ground motions tend to saturate over the magnitude range and strongly correlate with fault distance. As a result, this work can achieve the fault extent using seismic intensity and GMPE. We considered three types of fault models: point-source, line-source, and rectangle-source model. We found the most probable model parameters for each model by minimizing the residual sum of squares between the observed and estimated seismic intensities. The Akaike Information Criterion selected the most probable model among them. The strong motion data set of the 2008 Wenchuan, 2011 Tohoku, and 2016 Kumamoto earthquakes was used to test our methodology. The new method for estimating the fault geometry can obtain the ongoing rupture length and direction using the strong motion data. The model selection scheme with the Akaike Information Criterion selected the finite-source model to explain the shaking distribution. Results revealed that this new approach performed well in estimating the fault dimension. The method can promote the accuracy of the seismic intensity estimation for future large earthquakes, including the subduction earthquakes.

Keywords: Earthquake early warning, JMA seismic intensity, Real-time rupture estimation, Fault distance

*Correspondence: masumi@eqh.dpri.kyoto-u.ac.jp

³ Disaster Prevention Research Institute, Kyoto University, Gokasho, Uji, Kyoto 611-0011, Japan
Full list of author information is available at the end of the article



Introduction

Earthquake early warning (EEW) has attracted much research attention worldwide and implemented in earthquake-prone countries (Hoshiba et al. 2008; Wu 2014; Satriano et al. 2011; Allen et al. 2009; Chung et al. 2019). The EEW systems' ultimate goal is to estimate and inform the ground shaking at a location before or close to the onset of the strong shaking. Valid source determination is critical to achieving this. The traditional source determination approach determines the hypocenter location and magnitude from the early P-wave data (Kanamori 2005; Odaka et al. 2003; Allen and Kanamori 2003).

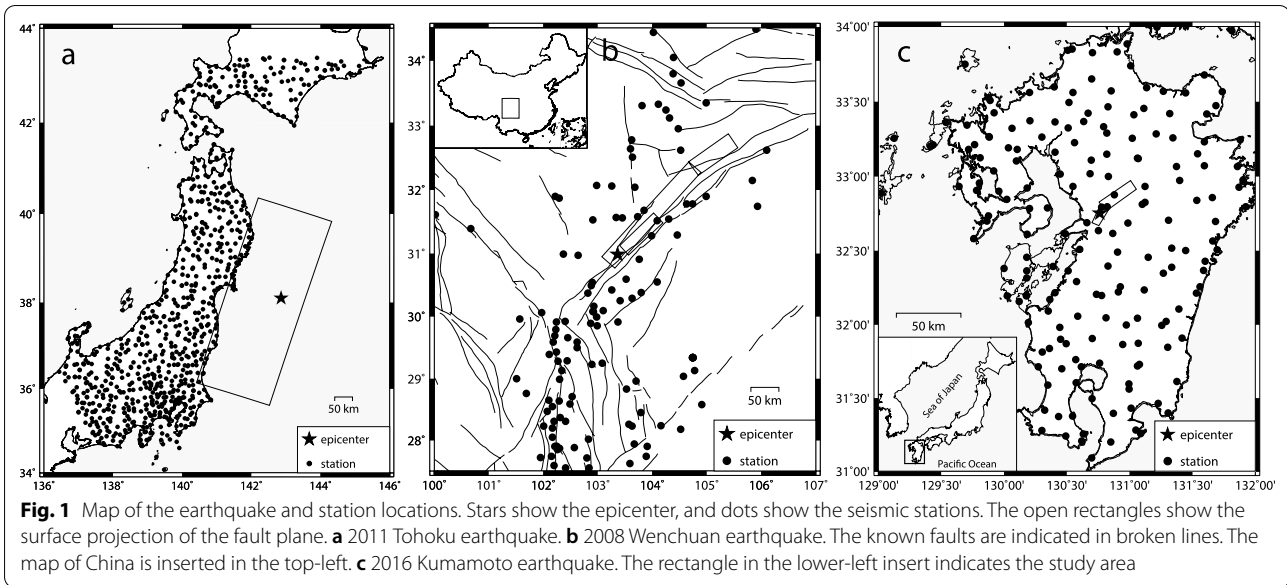
The point-source (PS) model estimates the shaking intensity at a site based on the estimated magnitude and location, assuming the shaking intensity decays as a function of the hypocenter distance (Odaka et al. 2003). This approach performs well in estimating shaking intensity for small-to-moderate earthquakes. However, the fault rupture length can be tens to hundreds of kilometers for large earthquakes. There are significant differences between hypocenter distances and fault-to-site distances (here-in-after referred to as fault distance) at distant stations. As a result, the ground-motion prediction equation (GMPE) with the PS model underestimates the shaking at stations around the fault but far away from the hypocenter. Consideration of the fault distance into the GMPE will improve the accuracy of the shaking intensity estimation.

Fault distance should be employed in this case for GMPE of large earthquakes instead of source-to-site distance. Several techniques for capturing the fault finiteness in real time and incorporating it into shaking

estimation have been developed. Yamada et al. (2007) established a method for classifying seismic records into near-source and far-source by identifying the fault geometry using peak ground acceleration (PGA) and velocity (PGV), assuming a dense seismic network around the fault. Convertito et al. (2012) also estimated the size of the rectangle-source (RS) model from PGA and PGV. The Finite-Fault Rupture Detector (FinDer) algorithm (Böse et al. 2012, 2015, 2018) computes rapid line-source models from template matching and is suited for small to large earthquakes (M2–M9) with rupture length ranging from less than one to several hundred kilometers. The FinDer uses templates precomputed from generic or local GMPEs for different line-source lengths.

The Propagation of Local Undamped Motion (PLUM) method (Kodera et al. 2018) predicts seismic intensities from observed real-time seismic intensities near target sites. Data assimilation techniques (Hoshiba and Aoki 2015) are also used in real-time shake mapping and wave propagation simulations. These methods do not require source estimation, but the warning time tends to be short compared with source-determination-based algorithms.

This study proposes a new methodology, XYtracker, which estimates the surface projection of the fault extent, and the Japan meteorological agency (JMA) seismic intensity scale (here-in-after referred to as seismic intensity) is used to describe the intensity of seismic shaking in Japan. As a result, directly converting continuous waveforms to the seismic intensity and estimating the maximum seismic intensity is easier. We used PS, line-source (LS), and RS models to track the real-time fault extent and obtained the model parameters by fitting the



observed seismic intensity. The Akaike information criterion (AIC) selects the most probable model among them. A PS model will be selected for small earthquakes, essentially the same as the current JMA EEW. We can perform the model selection and the model parameter estimate in a single framework.

Data

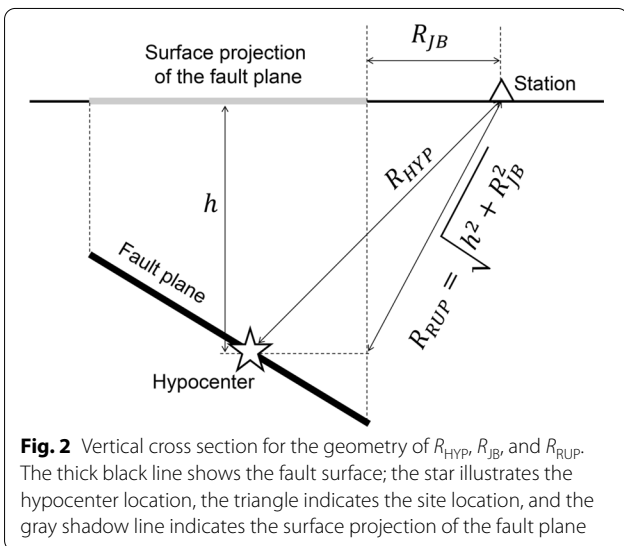
Strong motion data set

We used the 2011 Tohoku earthquakes (M_w 9.0) and the 2008 Wenchuan earthquake (M_w 8.0) for our simulation, since they feature a long rupture and good station coverage along the fault. We also performed the simulation

with the 2016 Kumamoto earthquake (M_{JMA} 7.1) as an example of a more minor inland earthquake.

The 2011 Tohoku earthquake occurred at 05:46 on March 11th, 2011 (UTC), offshore of the Tohoku region, Japan. The hypocenter location was determined as 38.10° N and 142.86° E at a depth of 24 km (Japan Meteorological Agency 2011). We used the strong motion data of the K-NET and KiK-net seismic networks (National Research Institute for Earth Science and Disaster Resilience 2019). It was a subduction-zone earthquake, and the station coverage was one-sided from the fault rupture (Fig. 1a). We selected the 831 stations with a hypocenter distance of <600 km. The fault model obtained from the joint inversion of the teleseismic body and surface waves (Shao et al. 2011) is shown as a rectangle. The fault size was about 500 times 100 km with a strike of 14°.

The 2008 Wenchuan earthquake was a crustal earthquake that occurred in the middle of the dense seismic network in Sichuan province, China. The earthquake occurred at 06:28:01 on May 12th, 2008 (UTC). The hypocenter location was estimated as 31.00° N and 103.32° E at a depth of 19 km (United States Geological Survey 2008). Data for this study were provided by China Digital Strong Motion Network (2008). The stations have a good azimuthal coverage along the fault, and the station density was about 40-km spacing (Fig. 1b). We used the 71 stations with the hypocenter distance <400 km. Because the data did not have the correct clock information, we adjusted the clock by assuming that the P-waves arrive at the theoretical arrival time calculated from the one-dimensional velocity structure (Shen et al. 2011). The finite-fault model in Fig. 1b was obtained from the



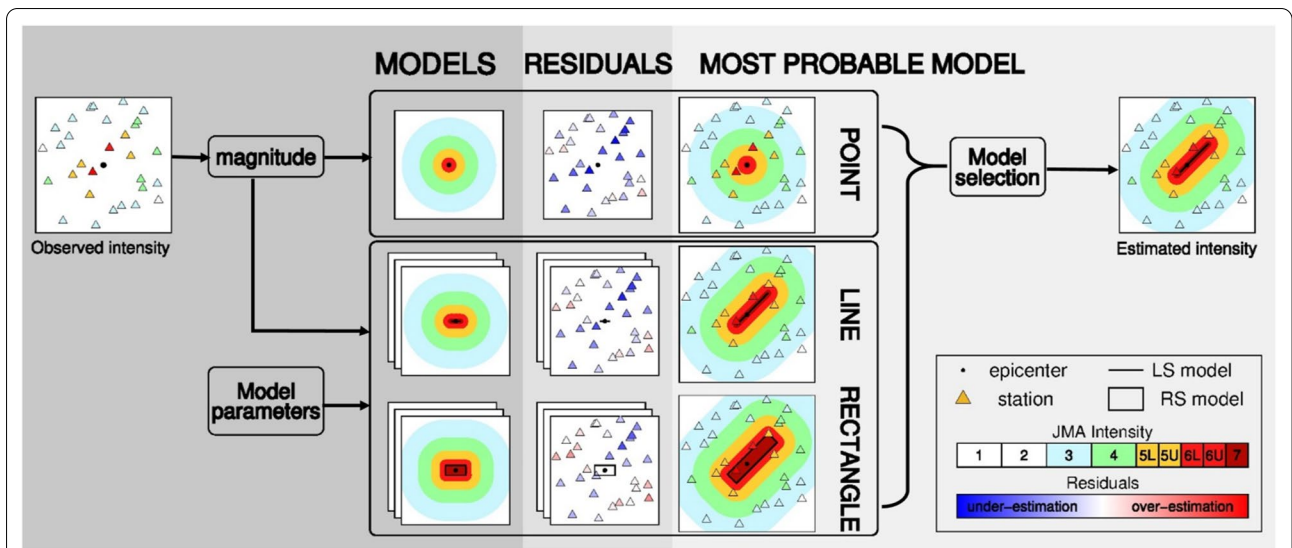


Fig. 3 Flow of XYtracker. The process comprises three steps: (1) obtaining source model parameters from the observed seismic intensity, (2) computing the residual between the observed and estimated intensities, and (3) selecting the most probable model based on AIC

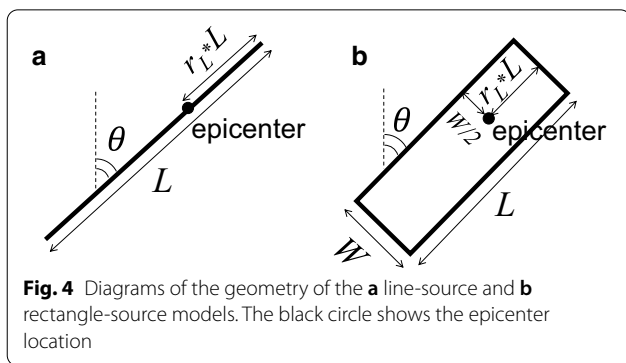


Fig. 4 Diagrams of the geometry of the **a** line-source and **b** rectangle-source models. The black circle shows the epicenter location

Table 1 Search range of the parameters for line- source and rectangle-source models

Parameter	L (length) [km]	W (width) [km]	θ (strike) [°]	r_L
Min	1	1	0	0
Max	$2V_r t$	L	180	1

joint inversion with the teleseismic waveforms and local coseismic displacement (Wang et al. 2008). The rupture was about 300 times 40 km along the Longmen Shan tectonic region, with a strike of 222° .

The 2016 Kumamoto earthquake ($M_{JMA}7.1$) was a crustal earthquake that occurred in the central part of Kyushu Island, southwest Japan. The station occurred at 16:25 on April 15th, 2016 (UTC). The hypocenter location was determined as 32.75° N and 130.76° E at a depth

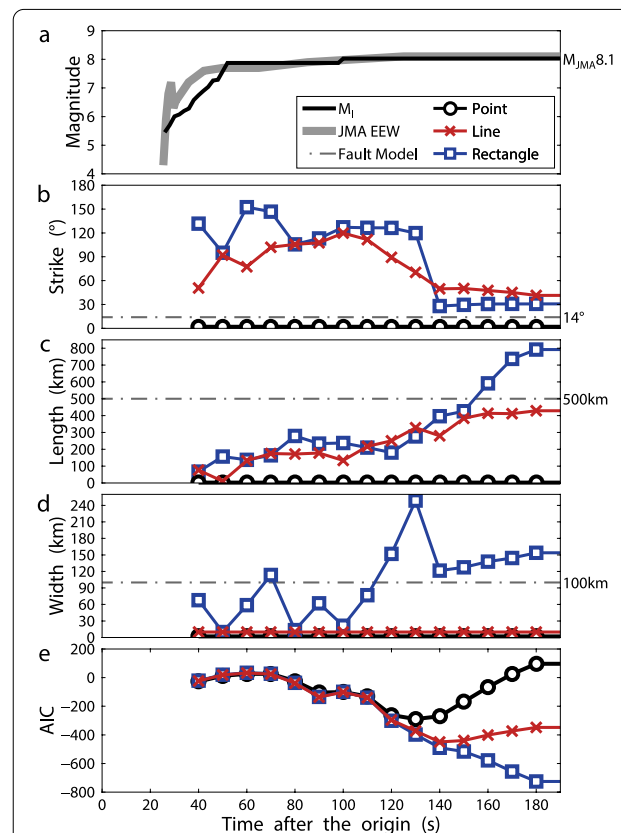
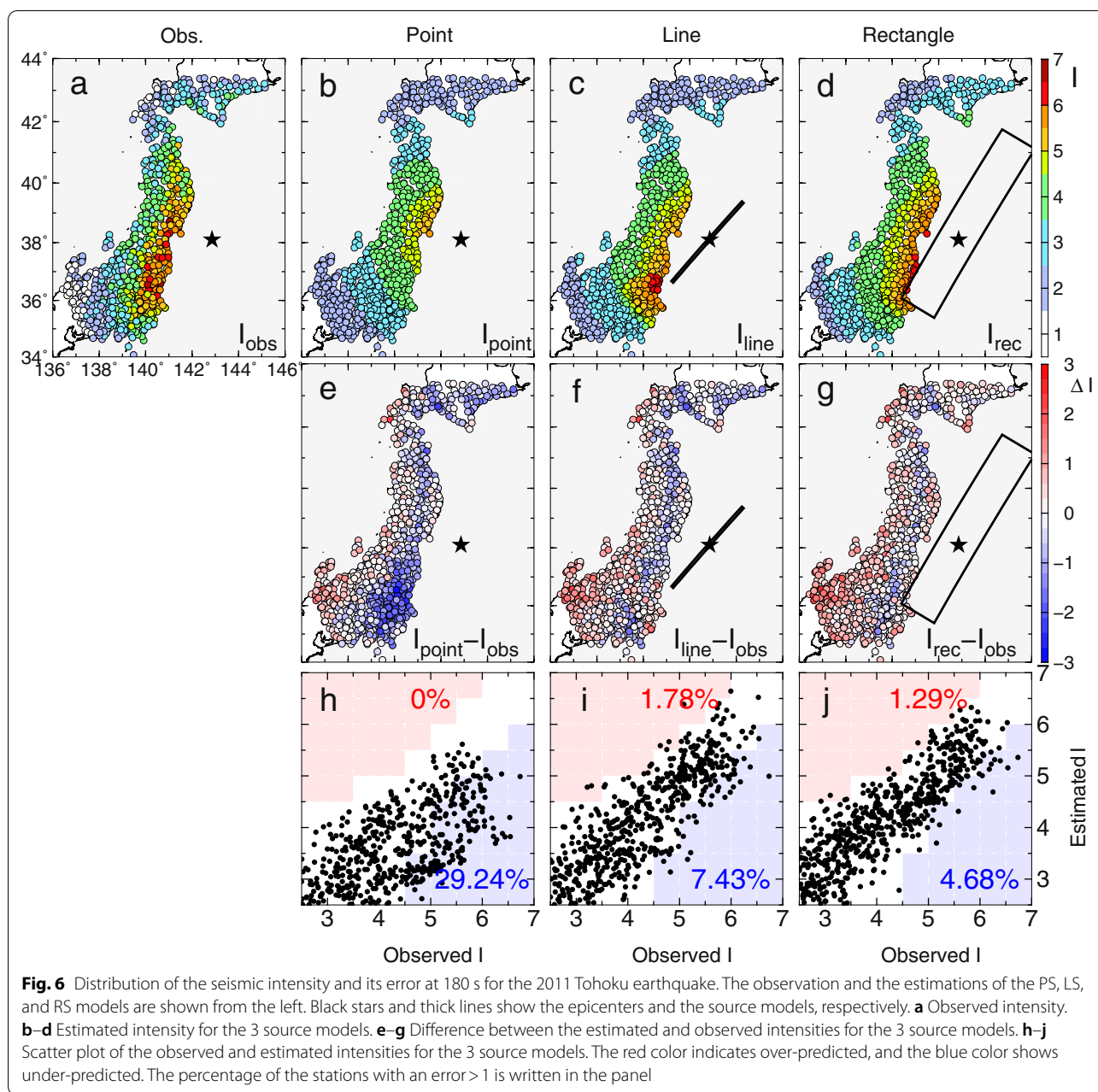


Fig. 5 Time history of the source parameters for the 2011 Tohoku earthquake. **a** Magnitude, **b** fault strike, **c** fault length, **d** fault width, and **e** AIC. In **a**, black and gray lines show the intensity magnitude and JMA EEW magnitude, respectively. **b–e** Black, red, and blue lines show the PS, LS, and RS models, respectively. The broken line shows the source model in Shao et al. (2011)



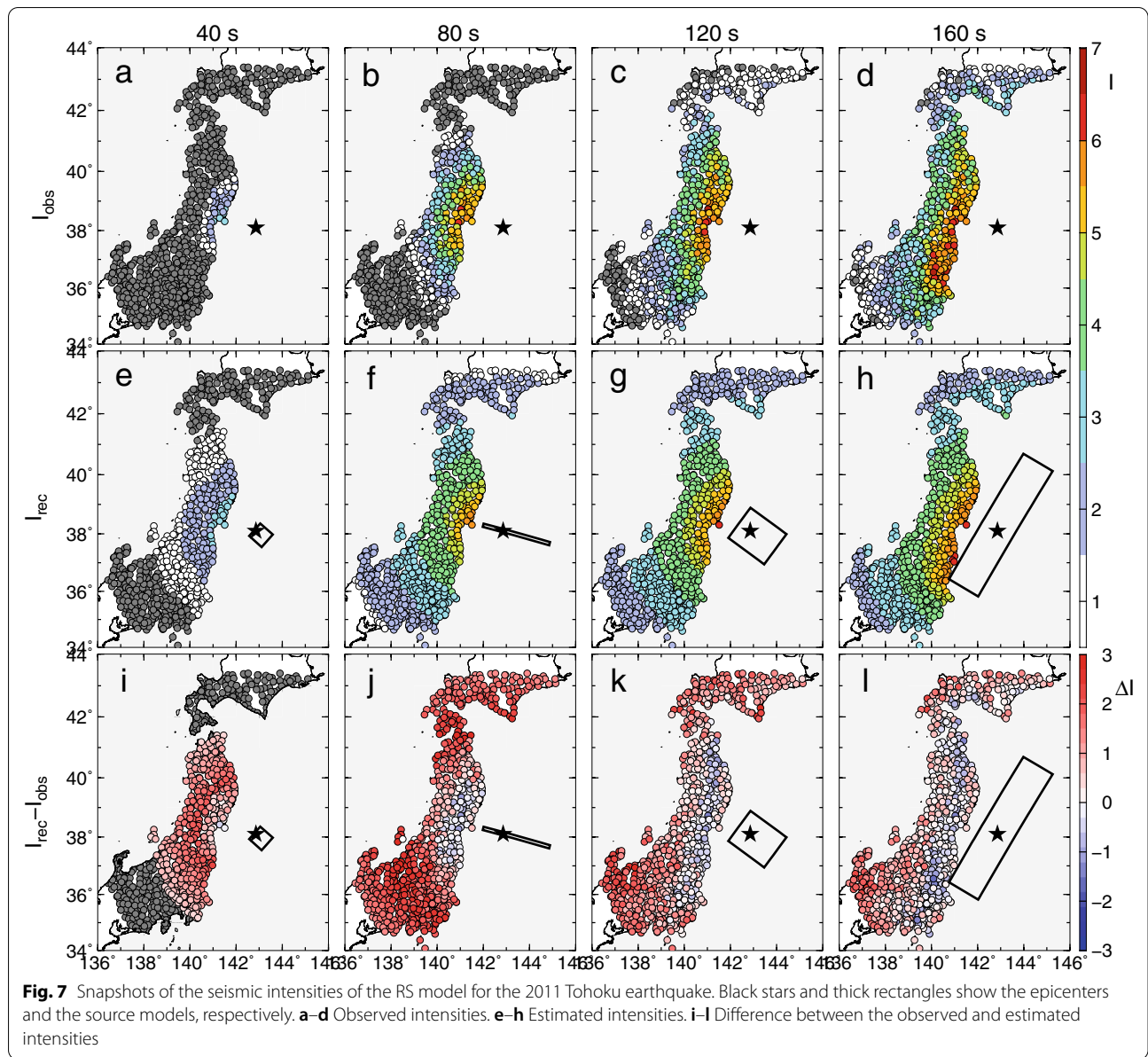
of 12 km. We used the strong motion data of the K-NET and KiK-net seismic networks processed by NIED, 390 stations with hypocenter distance < 400 km, as indicated in Fig. 1c was employed in this study. The fault model was obtained from the kinematic waveform inversion (Asano and Iwata 2016). The surface projection of the fault is shown in Fig. 1c.

The strong motion records of two earthquakes are all 3-component accelerograms. The sampling frequency of the data of the Tohoku earthquake and the Kumamoto

earthquake was 100 Hz, and that of the Wenchuan earthquake was 200 Hz. We processed the data in the following way: we subtracted the pre-event mean from the acceleration records. We then applied a recursive intensity filter to calculate the seismic intensity in real time. The detail of the filter will be explained in the next section.

Definition of the fault distance

The hypocenter distance (R_{HYP}) is the distance between the station and the hypocenter. R_{HYP} is utilized for the GMPE, assuming the PS model. We employed two



definitions for the fault distance to consider the fault finiteness, as shown in Fig. 2. Joyner and Boore (1981) defined the shortest distance between a site and surface projection of the fault plane as the Joyner–Boore distance (R_{JB}). The rupture distance (R_{RUP}) is the closest distance between a site and the three-dimensional rupture plane (Abrahamson and Silva 1997). A high-frequency ground motion is sensitive to R_{JB} but less sensitive to the dip of the fault plane (Yamada et al. 2007). Therefore, we presume the depth of the fault is constant at the hypocenter depth (h) and use $\sqrt{h^2 + R_{JB}^2}$ for the three-dimensional fault distance.

XYtracker method

The XYtracker is a new approach that considers the two-dimensional rupture for the seismic intensity estimation. It employs the GMPE of the shaking intensity as a function of intensity magnitude and fault distance. We propose a model selection analysis with the AIC to determine the most likely source model among PS, LS, and RS models. The processing flow is shown in Fig. 3.

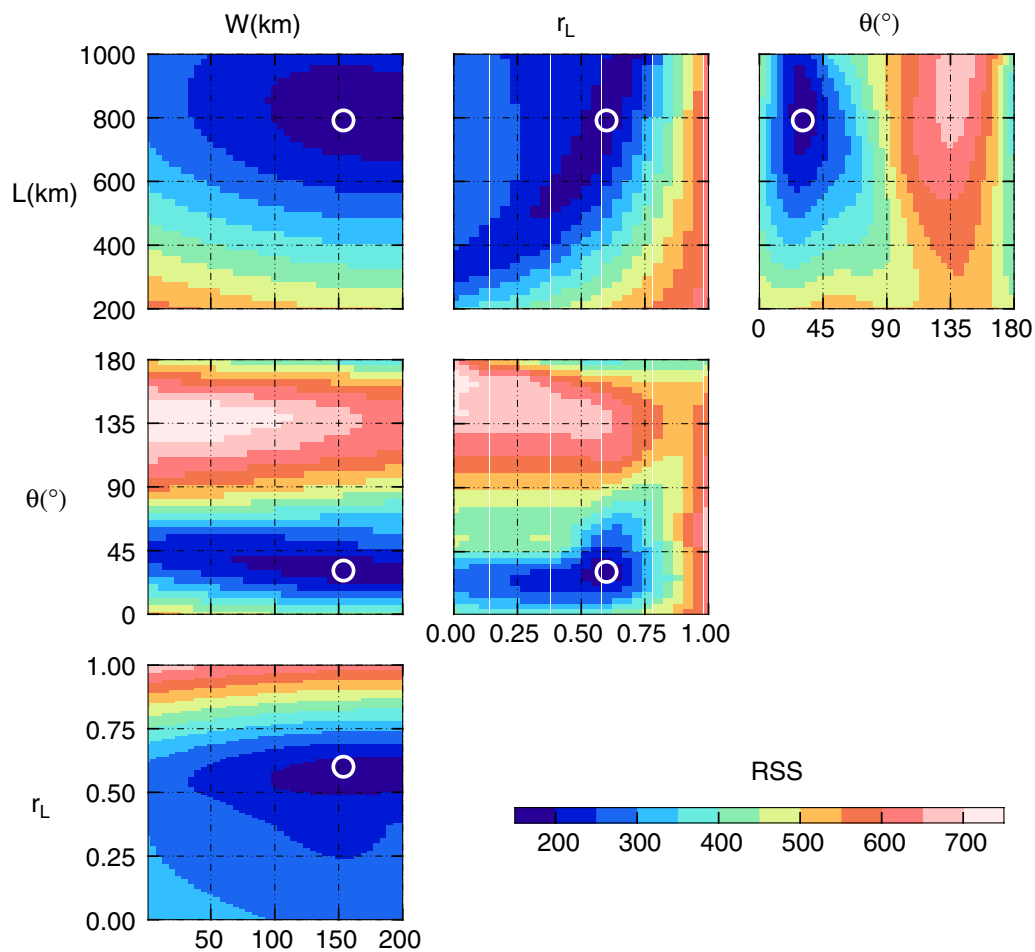


Fig. 8 Residual surface of the 4 model parameters (L , W , θ , and r_L) at 180 s after the origin time for the 2011 Tohoku earthquake. The color bar shows the values of RSS. White circles show the minimum RSS in each subfigure

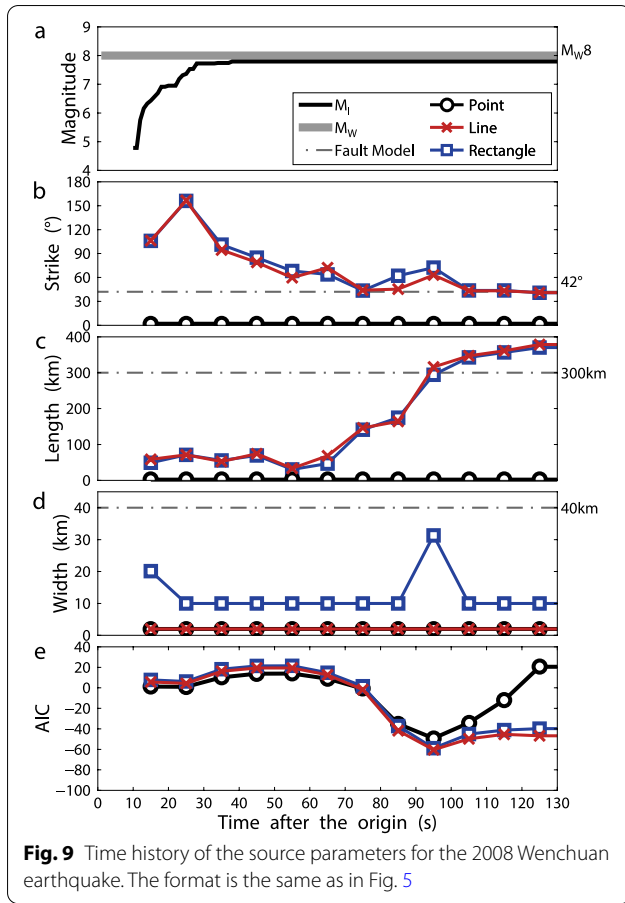
JMA seismic intensity

A high-frequency ground motion has a strong correlation with the fault distance and saturates over a large magnitude (Yenier and Atkinson 2015). As a result, it can estimate the fault distance and the fault geometry in real time (Izutani 1993; Yamada and Heaton 2008; Yamada et al. 2007).

In this study, we employed the seismic intensity to estimate the level of the high-frequency ground motions. We applied this ground motion measure, because it is used to express the level of shaking in Japanese EEW. Kunugi

et al. (2013) proposed a recursive filter to calculate the seismic intensity. The filter had a peak at around 1 s, and the filtered acceleration has a good correlation with the 1 s ground motion.

The JMA seismic intensity (I_{JMA}) can be computed from the filtered acceleration waveforms in each time step. After we applied the JMA seismic intensity filter (Kunugi et al. 2013), the vector sum of the three-component waveforms was calculated. Considering the absolute amplitude a_c having a total duration ≥ 0.3 s, the JMA seismic intensity is obtained by



$$I_{JMA} = 2 \log_{10}(a_c) + 0.94. \quad (1)$$

The real-time seismic intensity at each time step is calculated from Eq. (1).

Intensity magnitude

We employed the definition of the intensity magnitude (M_I) for the magnitude, which was a function of the JMA seismic intensity (I_{JMA}) and hypocenter distance. The uncertainty of the intensity estimated from the M_I was significantly lower than the intensity estimated from other conventional magnitudes (Yamamoto et al. 2008). M_I is expressed as a function of S-wave travel time (t_s), I_{JMA} , and R_{HYP} :

$$M_I = I_{JMA}/2 + \log_{10}(R_{HYP}) + at_s + b \quad (2)$$

where a and b are constants $a \approx 0.012$ and $b \approx 2.73$ (Yamamoto et al. 2008).

We utilize the median of the M_I obtained from the 5 closest stations from the hypocenter. Over time, the M_I

increased as the shaking intensity increased. The same equation will be used to estimate I_{JMA} at each site.

Source models

We considered fault finiteness by assuming two types of fault models: LS and RS models. Most of the EEW systems can detect the epicenter location soon after the earthquake occurs, so we assumed the location of the epicenter was identified from the first few P-wave arrivals. We constrained that the epicenter was included in the LS and RS models. The line model was parameterized by three parameters, length of the fault (L), the strike of the fault (θ), and the ratio of the length from the epicenter to one end along the strike (r_L). The RS model had an additional parameter, the width of the fault (W). We assumed that the epicenter was always at the center of the fault width to reduce the parameters. Figure 4 indicates the geometry of the LS and RS models.

We searched the most probable model parameters by minimizing the misfit function, defined by the residual sum of squares (RSS) between the observed and estimated seismic intensities:

$$RSS = 1/n \sum_{i=0}^n [I_i^{obs} - I_i^{est}]^2 * w_i \quad (3)$$

$$I^{est} = 2(M_I - \log_{10}(R_{RUP}) - at_s - b) \quad (4)$$

$$w_i = \begin{cases} 1 & I_i^{obs} \geq I_i^{point} \\ 2(I_i^{obs} - I_i^{point}) + 1 & I_i^{point} - 0.5 \leq I_i^{obs} \leq I_i^{point} \\ 0 & I_i^{obs} \leq I_i^{point} - 0.5 \end{cases} \quad (5)$$

where n is the number of the stations where the observed seismic intensity is larger than 2.5, I_i^{obs} is observed seismic intensity at the station i . w_i is a weight at the station i defined as Eq. (5). We use the weight to minimize the effect of the distant stations which have not reached their peak values. R_{RUP} is a hypocenter distance for the PS model but the fault distance for the LS and RS models. R_{RUP} for a finite source model is defined as $\sqrt{h^2 + R_{JB}^2}$ and R_{JB} is a function of model parameters (L, W, θ, r_L).

We searched the possible source parameters for LS and RS models that minimize the misfit function (Eq. (3)). The numerical optimization algorithm provided by Matlab has a good and fast service for the multidimensional optimization of model parameters (Nelder–Mead method). Table 1 shows the range of parameters for optimization. We assume a constant rupture velocity

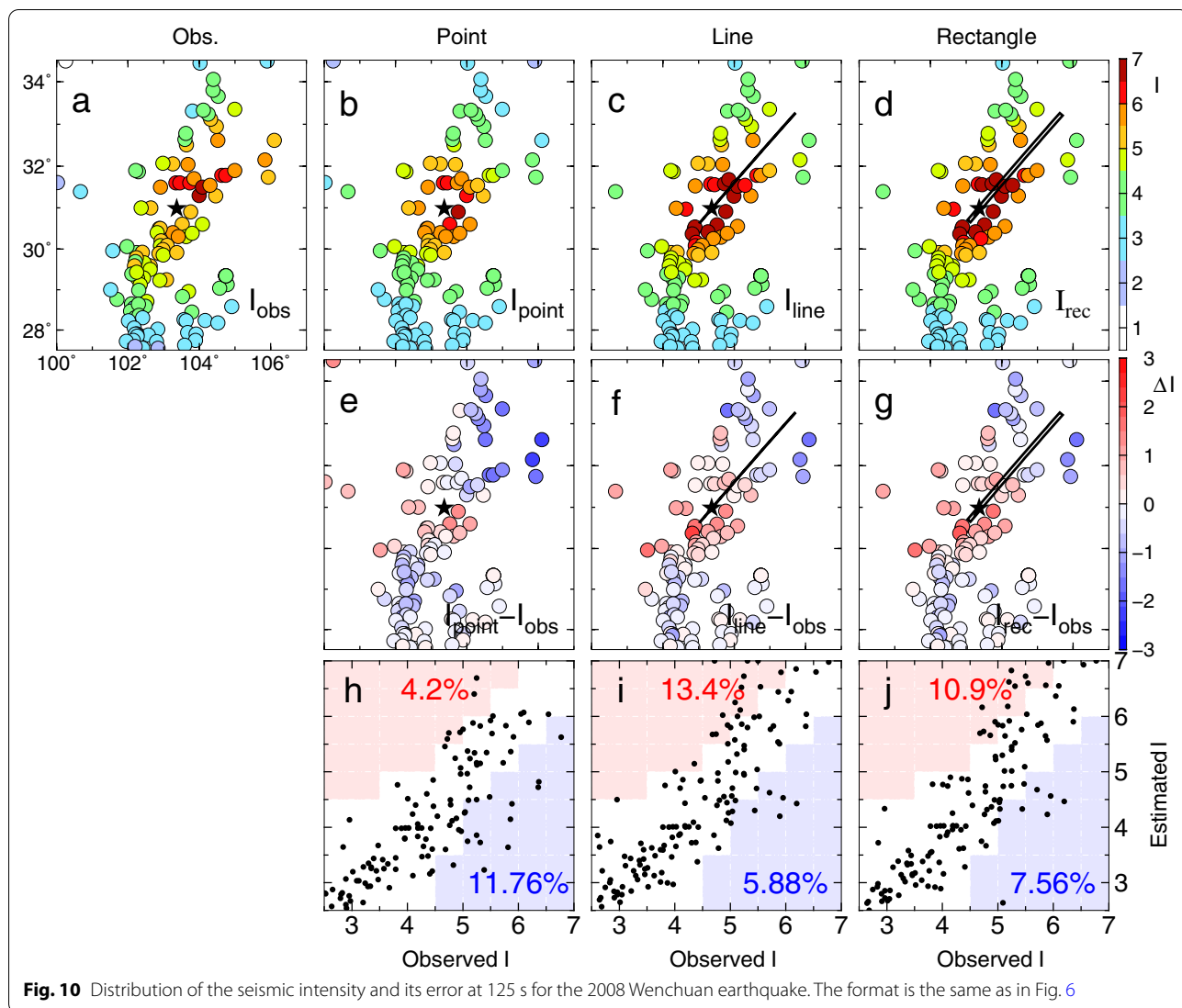


Fig. 10 Distribution of the seismic intensity and its error at 125 s for the 2008 Wenchuan earthquake. The format is the same as in Fig. 6

($V_r = 2.5$ km/s) and bilateral rupture along the strike; $t(s)$ is the time after the origin.

Model selection by AIC

We employed the AIC to select the most relevant source model among the PS, LS, and RS models (Akaike 1974). The AIC estimated the balance between the complexity of the models and the goodness of fit to the data:

$$AIC = 2k + n \ln(RSS) \tag{6}$$

where k represents the number of the free parameters and n also denotes the number of the stations where the observed seismic intensity is 2.5 or greater. We use $k=0, 3,$ and 4 for the PS, LS, and RS models.

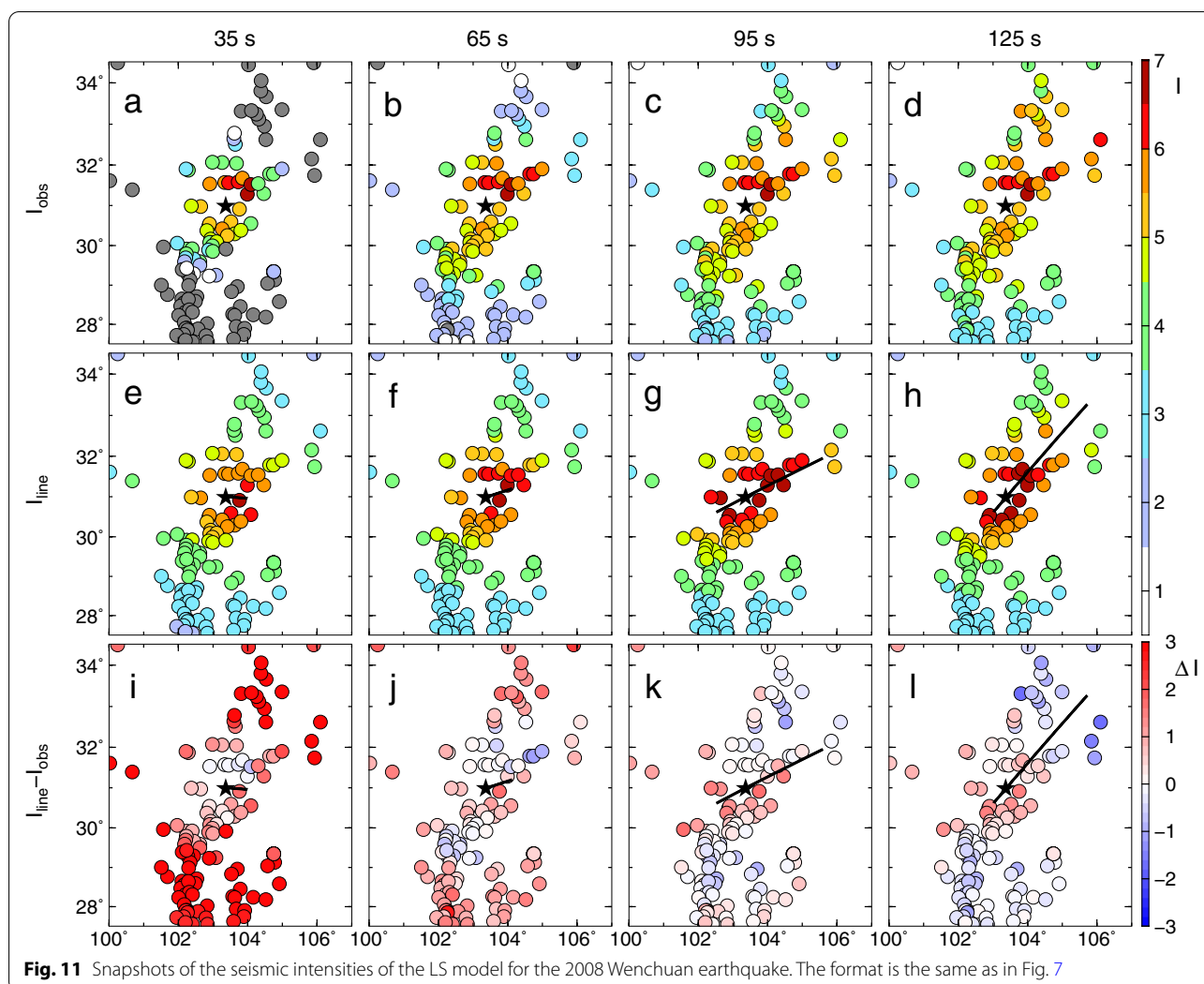
Results

We applied our novel source estimation algorithm to the 2011 Tohoku earthquake (M_w 9.0), the 2008 Wenchuan earthquake (M_w 8.0), and the 2016 Kumamoto earthquake (M_{JMA} 7.1). We used PS, LS, and RS models to describe the fault rupture extent and select the most probable model by AIC.

Results of the 2011 Tohoku earthquake

Comparison of the source models

Figure 5a shows the time history of the M_I and the JMA EEW magnitude for the 2011 Tohoku earthquake (Japan Meteorological Agency 2011). Although the definition of the magnitude was slightly different (JMA EEW



magnitude is computed from the high-pass filtered displacement), their trends were similar. Note that the magnitude estimated from the high-frequency ground motions saturates for large earthquakes; therefore, it underestimated the M_w (9.0). We used this time history of the intensity magnitude to estimate the source model parameters.

Figure 5b–d shows the most probable source parameters for the LS and RS models. The fault length keeps increasing as the rupture propagates. Because it was an offshore earthquake and the station coverage was one-sided from the epicenter, it took about 140 s to obtain the stable strike. Figure 5e shows the time history of the AIC for three source models. The difference between the PS

and finite-source became significant after 120 s, and the fault width became profound after 140 s.

Figure 6 shows the spatial distribution of the observed and estimated intensities. The high intensities were observed along the east coast of the Tohoku region (Fig. 6a). LS and RS models could reproduce this directivity of the strong shaking. PS model significantly underestimated the seismic intensity in the Tokyo region (Fig. 6e). Assuming that the intensity error within the ± 1 scale is acceptable, the accuracy for the PS model was 71%, and that for the LS and RS models were 91% and 94%, respectively. These results are consistent with the model selection by the AIC (Fig. 5e).

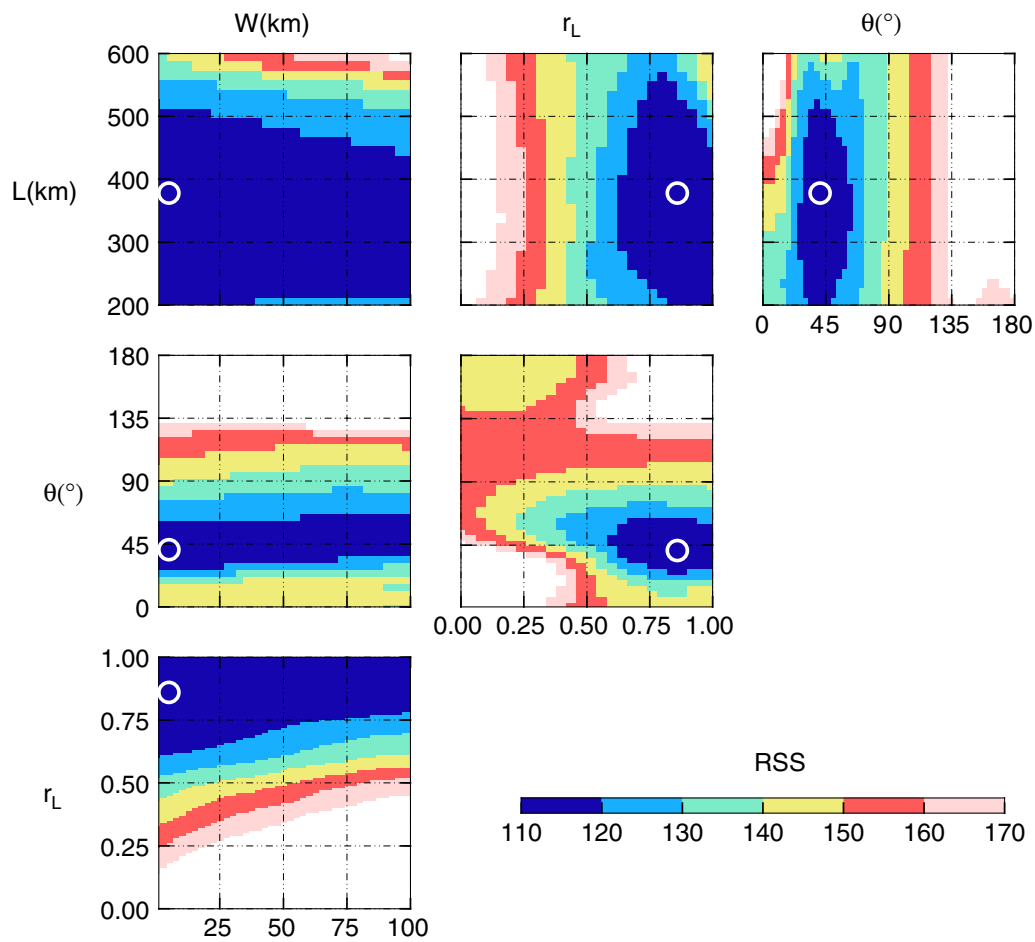


Fig. 12 Residual surface of the four model parameters (L , W , θ , and r_L) at 125 s after the origin time for the 2008 Wenchuan earthquake. The format is the same as in Fig. 8

Performance of the optimal source model

Figure 7 shows the snapshots of the seismic intensities of the RS model for the 2011 Tohoku earthquake at 40, 80, 120, and 160 s after the origin time. At 40 s, the observed intensity distribution was isotropic primarily, and the RS model was close to the PS model. The estimated shaking intensity was larger than the observation at the stations far from the source, which suggests that the EEW can be effective in that area. The directivity of the shaking intensity distribution was not apparent until 120 s. At 160 s, the estimated model was almost converged, and the bilateral rupture in the NNE–SSW direction was captured.

We checked the sensitivity of the model parameters to the misfit function. Figure 8 shows the residual surface of

the RS model after the convergence. Combinations of 2 out of 4 model parameters are plotted in each subfigure. Length, strike, and the length of the one side from the epicenter (r_L , L) are well constrained, but the width has a considerable variation. Since station distribution is one-sided from the fault, the method does not have a good resolution for the width of the fault.

Results of the 2008 Wenchuan earthquake

Comparison of the source models

We performed the same simulation with the data set of the 2008 Wenchuan earthquake. Figure 9a shows the time history of the M_I and final M_w (8.0). The M_I

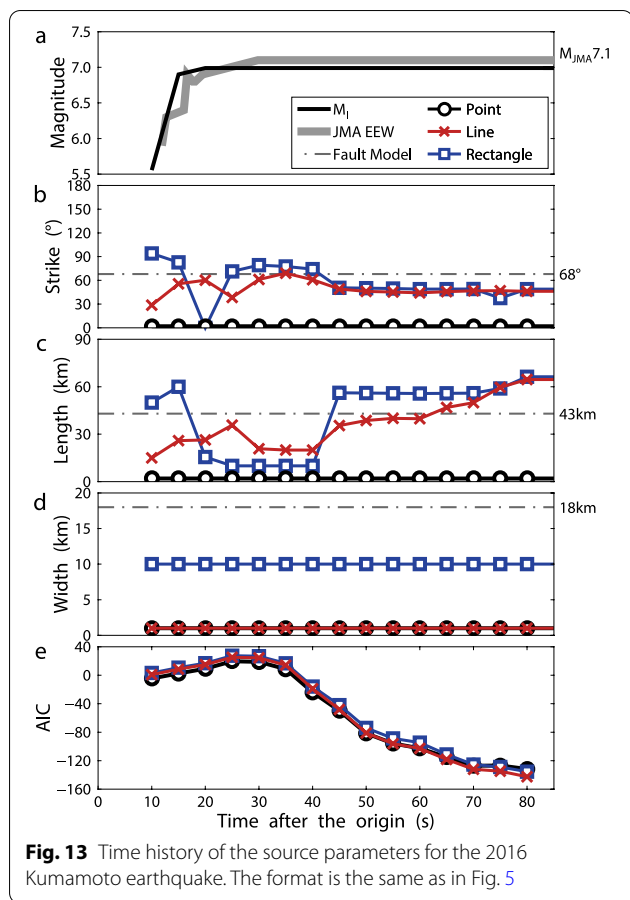


Fig. 13 Time history of the source parameters for the 2016 Kumamoto earthquake. The format is the same as in Fig. 5

increased for the first 30 s and converged to 7.8. Owing to the difference in the definition, the M_I underestimates the M_w .

Figure 9b–d shows the time histories of the most probable source parameters. The length started increasing at 70 s after the origin time, and the fault finiteness became important. The final length is very similar to the fault model from the waveform inversion (Wang et al. 2008). Unlike the 2011 Tohoku earthquake, the width of the RS model is minimal. This is consistent with the very narrow surface projection of the source model in Fig. 1b.

Because the fault rupture extent is very narrow, there is not much difference in the LS and RS models (Fig. 10c, d). Therefore, the AIC selected the LS model, because it had fewer parameters than the RS model.

Performance of the optimal source model

Figure 11 shows the snapshot of the seismic intensities of the LS model for the Wenchuan earthquake at 35, 65,

95, and 125 s after the origin time. At 35 s, the observed intensity distribution was isotropic, and the estimated model was similar to the PS model. The estimated intensity was larger than the observations at the distant stations, and we could have provided tens of warning time. The estimated intensity At 95 s, the directivity of the shaking distribution became apparent, and the LS started capturing the fault direction.

Figure 12 shows the residual surface of the model parameters for the 2008 Wenchuan earthquake. Although the AIC selected the LS model as the best model, we showed the residual surface of the RS model here, because the LS model is a subset of the RS model. Resolutions for r_L and θ are better than L and W , probably due to the heterogeneity of the station distribution.

Results of the 2016 Kumamoto earthquake

Comparison of the source models

Figure 13a shows the time history of M_I and the JMA EEW magnitude for the 2016 Kumamoto earthquake. M_I is similar to the JMA EEW magnitude and converges within the first 10 s after the first P-wave arrival.

Figure 13b–d shows the most probable source parameters for the LS and RS models. We can estimate the strike for the LS and RS models at the early rupture stage. The length of the RS model is slightly larger than that of the source model in Asano and Iwata (2016). There was an M5-class triggered earthquake in the Oita prefecture about 30 s after the mainshock and our method included it in the mainshock rupture. The width of the RS model is relatively narrow so the RS model is similar to the LS model. The AIC shown in Fig. 13e selected the LS model as the best model for the 2016 Kumamoto earthquake.

Figure 14 shows the final seismic intensity distribution for the 2016 Kumamoto earthquake. Although the LS model was selected as the best model by the AIC, the differences in the estimated intensities were tiny. The size of the earthquake ($M_{JMA} 7.1$) was not large enough to capture the fault rupture dimension by the finite-source model.

Performance of the optimal source model

Figure 15 shows the snapshot of the observed and estimated intensities of the LS model for the Kumamoto earthquake at 10, 30, 50, and 70 s after the origin time. At 10 s, the estimated intensity distribution (Fig. 15e) is similar to the final observed intensity distribution (Fig. 15d). The EEW would provide enough warning time on the entire Koshu island.

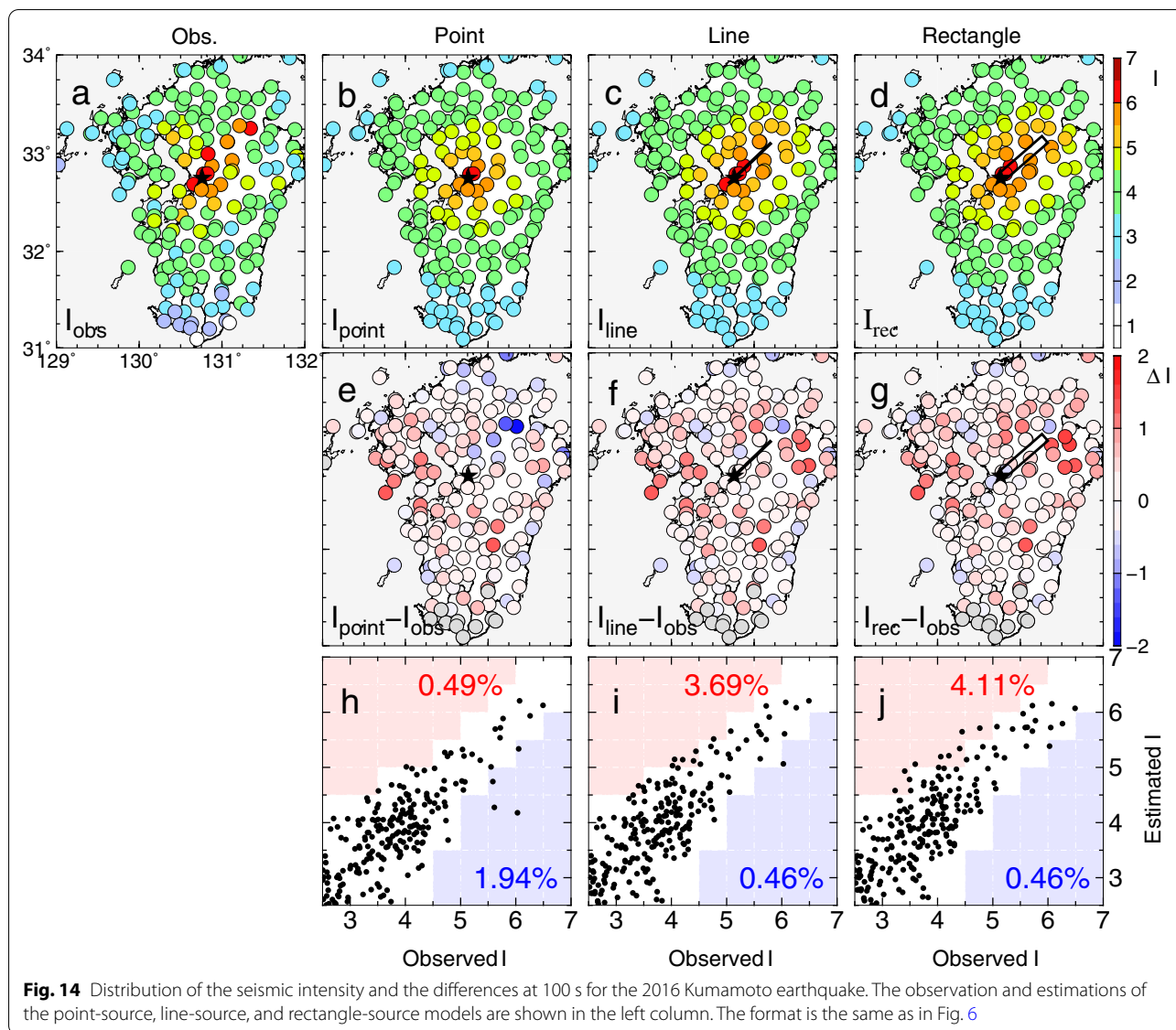


Figure 16 shows the residual surface of the model parameters for the 2016 Kumamoto earthquake. Although the AIC selected the LS model as the best model, we showed the residual surface of the RS model here, because the LS model is a subset of the RS model. All parameters were well-constrained.

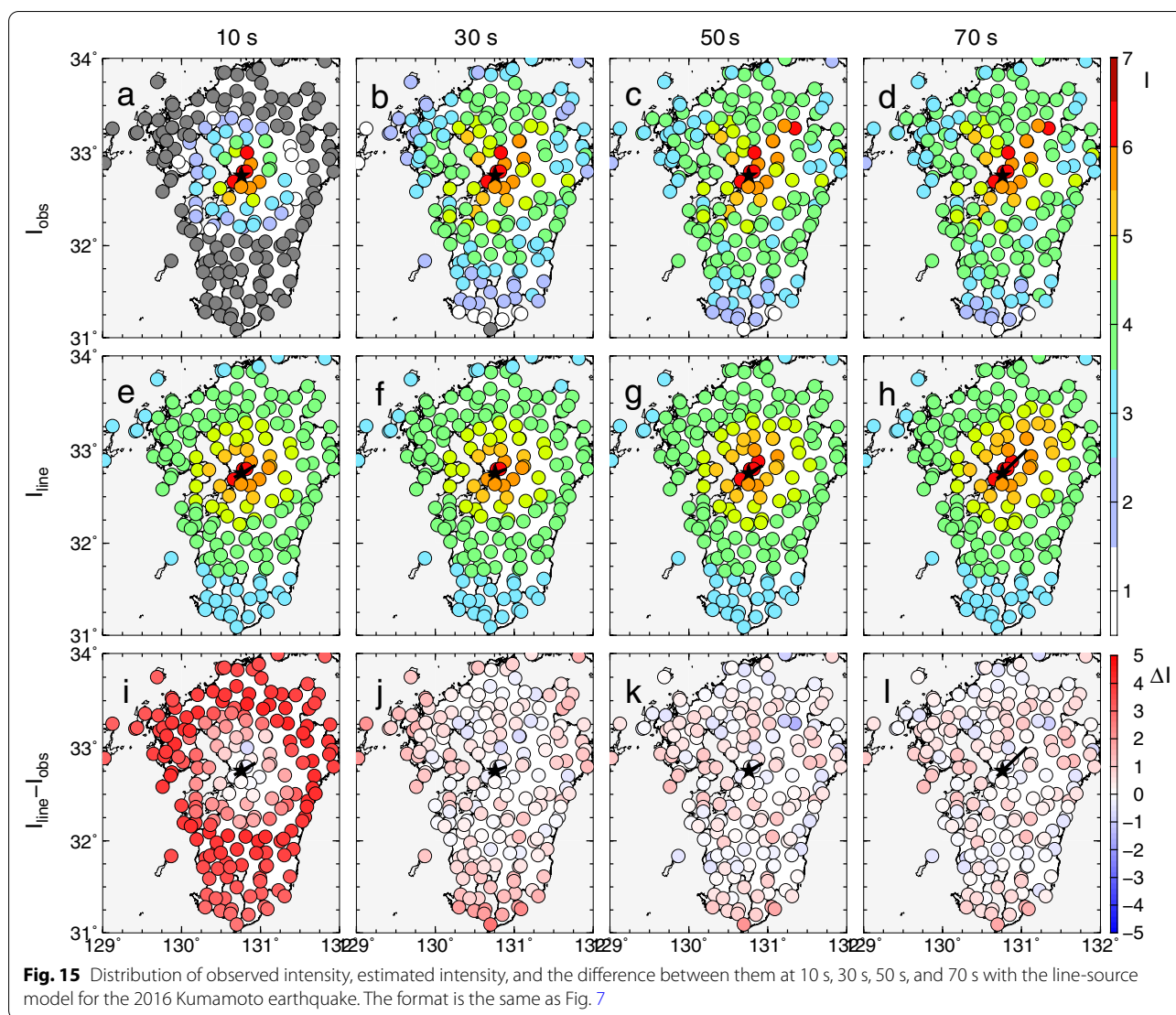
Discussion

Contribution to the earthquake early warning

This study proposed a methodology for estimating the rupture extent in real time from strong-motion recordings during shaking. LS, RS, and the conventional PS

model were examined in this study, and the AIC was used to select the best model that described the observed shaking intensity. Using a simple finite-source model, the accuracy of seismic intensity estimation was improved (Figs. 6 and 10).

Intensity magnitudes (M_I) computed from the real-time JMA seismic intensity were used instead of the moment magnitude. The Tohoku and Wenchuan earthquake’s rupture duration was 2–3 min, and the convergence of M_I for the two earthquakes was about 50 s and 30 s, respectively (Figs. 5 and 9). The M_I was estimated from the peak SI of the closest 5 stations so it converged



after the peak of the amplitude. However, the high-frequency ground motions saturate for large earthquakes, which may underestimate the moment magnitude. For the Tohoku case, M_I underestimated the moment magnitude (M_w 9.0).

The advantage of XYtracker is that it can handle both small and large earthquakes in a single framework. The AIC performs a model selection from the PS, LS, and RS models. Therefore, the PS model was selected at the early rupture stage for the three earthquakes (Figs. 5, 9, and 13). We use not only near-source stations but also far-source stations through the GMPE to estimate the rupture extent so that it can be applied for offshore

earthquakes. The XYtracker uses intensity magnitude, computed directly from the seismic intensity. This magnitude can decrease the uncertainty of the intensity estimation compared with the other conventional magnitudes.

The FinDer method has also been applied to both the Tohoku (Böse et al. 2012) and Wenchuan (Li et al. 2020) earthquakes. The method uses template matching, which requires precomputed templates from generic or local GMPEs for different line-source lengths. The major difference between our approach and the FinDer algorithm is the consideration of the fault width. For the narrow fault earthquakes, such as Kumamoto and Wenchuan earthquakes, both methods work well (Figs. 9e and 13e).

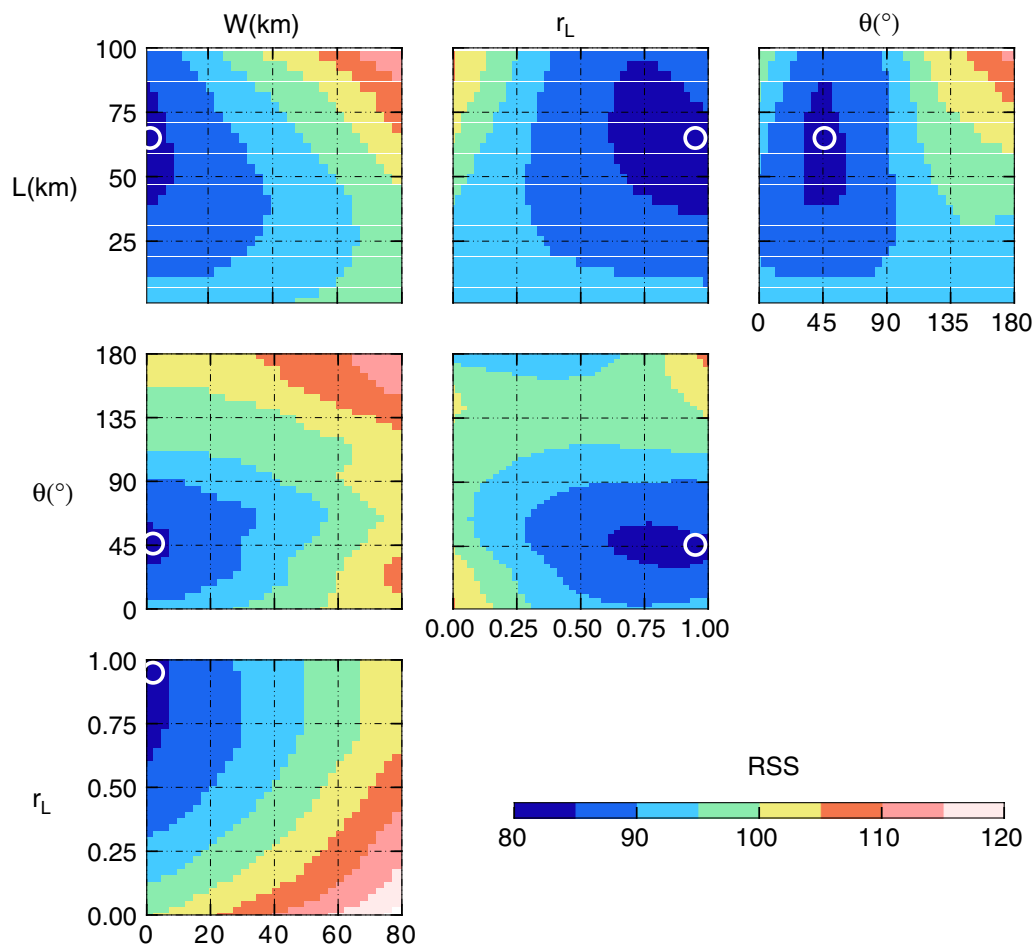


Fig. 16 Residual surface of the four model parameters (L , W , θ , and r_L) at 100 s after the origin time for the 2016 Kumamoto earthquake. The format is the same as Fig. 8

However, for large earthquakes with a wide fault, such as subduction earthquakes, consideration of the fault width will improve the shaking estimation. For the Tohoku earthquake, although the width estimation was not well constrained, the AIC selected the RS model to demonstrate the better shaking intensity (Fig. 5e). For wide fault and good station coverage, fault width will improve the shaking estimation.

The method uses stations where a strong motion has arrived to maintain track of the surface projection of fault. Therefore, it does not aim to predict the future evolution of the fault rupture. It is difficult to estimate the rupture direction until it evolves. The method is subject to the same limitations as other EEW methods. There will be a blind zone (i.e., no warning time) near the

hypo-center. The dense seismic station is required to estimate the rupture dimension accurately.

Future improvements

To estimate the fault distance from the observed seismic intensity, we use the GMPE for the intensity magnitude (Yamamoto et al. 2008). The equation was derived before the three earthquakes; therefore, these data were not included in the regression analysis. The data used for GMPE regression analysis is M_{JMA} 3.5 to 7.9, and there is no earthquake with a magnitude greater than 8. As a result, applying to megathrust earthquakes is an extrapolation of this equation. To improve the fault rupture estimation, it is good to create a GMPE from the data set of the large earthquakes whose rupture extent is challenging

to be approximated by a point source. Adding a site correction factor will also improve the shaking estimation.

This study demonstrated the offline simulation with three large earthquakes and showed that the new method would improve the intensity estimation. However, we need to test with a larger number of earthquakes to enforce and confirm the method's robustness. The method has a perspective to improve the estimation of the real-time seismic intensity.

Conclusions

We proposed the XYtracker method to estimate real-time seismic intensities using a finite source model. The LS and RS models, together with the conventional PS model, were examined in this study, and the AIC was used to select the best model that described the observed shaking intensity. Using a simple finite-source model improved the accuracy of seismic intensity estimation. By estimating the fault rupture dimension, we can use the fault distance instead of the epicenter distance for the GMPEs, which improves the estimation of the seismic intensity for large earthquakes.

Strong motion data of the 2011 Tohoku earthquake (M_w 9.0), 2008 Wenchuan earthquake (M_w 8.0), and the 2016 Kumamoto earthquake (M_{JMA} 7.1) were applied to examine the method. The AIC selected the PS model at the start of the rupture and then switched to the finite-source model as the rupture propagated. The RS model was selected for the 2011 Tohoku earthquake, with a wide fault of about 100 km. The LS model was selected for the 2008 Wenchuan and 2016 Kumamoto earthquakes.

The XYtracker method has the potential to improve the underestimation of the current EEW system for large earthquakes by considering the dimension of the rupture extent. The method can improve the accuracy of the seismic intensity estimation for future large earthquakes, including the subduction earthquakes.

Acknowledgements

We thank the JMA, NIED, and China Digital Strong Motion Network to install the seismic network and provide the data. We also acknowledge the National Key R&D Program of China and the China Scholarship Council for their financial support.

Author contributions

MY established the main method and XY analyzed the data and performed the simulation. Both authors participated in drafting the manuscript. All authors read and approved the final manuscript.

Funding

This research is supported by the National Key R&D Program of China (Grant No. 2018YFC1504004) and Seismology TowArd Research innovation with data of Earthquake Project by the Ministry of Education, Culture, Sports, Science and Technology, Japan. The China Scholarship Council (CSC) supported the visit of Xiao Ying (No. 201804190045) to the Disaster Prevention Research Institute, Kyoto University.

Availability of data and materials

The strong motion data for the 2011 Tohoku and 2016 Kumamoto earthquakes are available in NIED K-NET, KiK-net, National Research Institute for Earth Science and Disaster Resilience (<https://doi.org/10.17598/NIED.0004>). The strong motion data for the 2008 Wenchuan earthquake were provided by China Digital Strong Motion Network on request.

Declarations

Ethics approval and consent to participate

Not applicable.

Consent for publication

Not applicable.

Competing interests

The authors declare that they have no competing interests.

Author details

¹Key Laboratory of Earthquake Engineering and Engineering Vibration, Institute of Engineering Mechanics, China Earthquake Administration, Harbin, China. ²Key Laboratory of Earthquake Disaster Mitigation, Ministry of Emergency Management, Harbin, China. ³Disaster Prevention Research Institute, Kyoto University, Gokasho, Uji, Kyoto 611-0011, Japan.

Received: 3 March 2022 Accepted: 16 May 2022

Published online: 26 May 2022

References

- Abrahamson NA, Silva WJ (1997) Empirical response spectral attenuation relations for shallow crustal earthquakes. *Seismol Res Lett* 68(1):94–127. <https://doi.org/10.1785/gssrl.68.1.94>
- Akaike HT (1974) A new look at the statistical model identification. *IEEE Trans Autom Control* 19(6):716–723. <https://doi.org/10.1109/TAC.1974.1100705>
- Allen RM, Kanamori H (2003) The potential for earthquake early warning in southern California. *Science* 300(5620):786–789. <https://doi.org/10.1126/science.1080912>
- Allen RM, Gasparini P, Kamigaichi O, Böse M (2009) The status of earthquake early warning around the world: an introductory overview. *Seismol Res Lett* 80(5):682–693. <https://doi.org/10.1785/gssrl.80.5.682>
- Asano K, Iwata T (2016) Source rupture processes of the foreshock and mainshock in the 2016 Kumamoto earthquake sequence estimated from the kinematic waveform inversion of strong motion data. *Earth Planets Space* 68(1):147. <https://doi.org/10.1186/s40623-016-0519-9>
- Böse M, Heaton TH, Hauksson E (2012) Real-time finite fault rupture detector (FinDer) for large earthquakes. *Geophys J Int* 191(2):803–812. <https://doi.org/10.1111/j.1365-246X.2012.05657.x>
- Böse M, Felizardo C, Heaton TH (2015) Finite-fault rupture detector (FinDer): going real-time in californian shake alert warning system. *Seismol Res Lett* 86(6):1692–1704. <https://doi.org/10.1785/0220150154>
- Böse M, Smith DE, Felizardo C, Meier MA, Heaton TH, Clinton JF (2018) FinDer vol 2: improved real-time ground-motion predictions for M2–M9 with seismic finite-source characterization. *Geophys J Int* 212(1):725–742. <https://doi.org/10.1093/gji/ggx430>
- China Digital Strong Motion Network (2008) www.csmnc.net.cn. Accessed May 2017 (limited access).
- Chung AI, Henson I, Allen RM (2019) Optimizing earthquake early warning performance: elarmS-3. *Seismol Res Lett* 90(2A):727–743. <https://doi.org/10.1785/0220180192>
- Convertito V, Caccavale M, De Matteis R, Emolo A, Wald D, Zollo A (2012) Fault extent estimation for near-real-time ground-shaking map computation purposes. *Bull Seismol Soc Am* 102(2):661–679. <https://doi.org/10.1785/0120100306>
- Hoshiba M, Aoki S (2015) Numerical shake prediction for earthquake early warning: data assimilation, real-time shake mapping, and simulation of

- wave propagation. *Bull Seismol Soc Am* 105(3):1324–1338. <https://doi.org/10.1785/0120140280>
- Hoshiba M, Kamigaichi O, Saito M, Sy T, Hamada N (2008) Earthquake early warning starts nationwide in Japan. *Eos, Trans Am Geophys Union*. <https://doi.org/10.1029/2008eo080001>
- Izutani Y (1993) Fault length and direction of rupture propagation for the 1993 Kushiro-Oki earthquake as derived from strong motion duration. *J Phys Earth* 41:319–325
- Japan Meteorological Agency (2011) https://www.data.jma.go.jp/svd/eew/data/nc/pub_hist/2011/03/20110311144640/content/content_out.html. Accessed May 2022.
- Joyner WB, Boore DM (1981) Peak horizontal acceleration and velocity from strong-motion records including records from the 1979 Imperial Valley. *Bull Seismol Soc Am* 71(6):2011–2038. <https://doi.org/10.1785/BSSA0710062011>
- Kanamori H (2005) Real-time seismology and earthquake damage mitigation. *Annu Rev Earth Planet Sci* 33(1):195–214. <https://doi.org/10.1146/annurev.earth.33.092203.122626>
- Kodera Y, Yamada Y, Hirano K, Tamaribuchi K, Adachi S, Hayashimoto N, Morimoto M, Nakamura M, Hoshiba M (2018) The propagation of local undamped motion (PLUM) method: a simple and robust seismic wave-field estimation approach for earthquake early warning. *Bull Seismol Soc Am* 108(2):983–1003. <https://doi.org/10.1785/0120170085>
- Kunugi T, Aoi S, Nakamura H, Suzuki W, Morikawa N, Fujiwara H (2013) An improved approximating filter for real-time calculation of seismic intensity. *Seismol Soc Jpn 2nd Ser (zisin)*. 65(3):223–230. <https://doi.org/10.4294/zisin.65.223>
- Li J, Böse M, Wyss M, Wald DJ, Hutchison A, Clinton JF, Wu Z, Jiang C, Zhou S (2020) Estimating rupture dimensions of three major earthquakes in Sichuan China, for early warning and rapid loss estimates. *Bull Seismol Soc Am* 110(2):920–936. <https://doi.org/10.1785/0120190117>
- National Research Institute for Earth Science and Disaster Resilience (2019), NIED K-NET, KIK-net, National Research Institute for Earth Science and Disaster Resilience, <https://doi.org/10.17598/NIED.0004>.
- Odaka T, Ashiya K, Tsukada S, Sato S, Ohtake K, Nozaka D (2003) A new method of quickly estimating epicentral distance and magnitude from a single seismic record. *Bull Seismol Soc Am* 93(1):526–532
- Satriano C, Wu Y-M, Zollo A, Kanamori H (2011) Earthquake early warning: concepts, methods and physical grounds. *Soil Dyn Earthq Eng* 31(2):106–118. <https://doi.org/10.1016/j.soildyn.2010.07.007>
- Shao G, Li X, Ji C, Maeda T (2011) Focal mechanism and slip history of the 2011 M w 9.1 off the Pacific coast of Tohoku Earthquake, constrained with teleseismic body and surface waves. *Earth Planets Space* 63(7):559–564. <https://doi.org/10.5047/eps.2011.06.028>
- Shen XZ, Mei XP, Yang H (2011) Study on the crustal structures beneath Wenchuan earthquake rupture zone. *Prog Geophys*. <https://doi.org/10.3969/j.issn.1004-2903.2011.02.012> (in Chinese)
- United States Geological Survey (2008) <https://earthquake.usgs.gov/earthquakes/eventpage/usp000g650/executive>. Accessed May 2022.
- Wang WM, Zh L, Li J, Yao Z (2008) Rupture process of the Ms 8.0 Wenchuan earthquake of Sichuan China. *China Chinese J Geophys* 51(5):1403–1410. <https://doi.org/10.3321/j.issn:0001-5733.2008.05.013> (in Chinese)
- Wu Y-M (2014) Progress on development of an earthquake early warning system using low-cost sensors. *Pure Appl Geophys* 172(9):2343–2351. <https://doi.org/10.1007/s00024-014-0933-5>
- Yamada M, Heaton T (2008) Real-time estimation of fault rupture extent using envelopes of acceleration. *Bull Seismol Soc Am* 98(2):607–619. <https://doi.org/10.1785/0120060218>
- Yamada M, Heaton T, Beck J (2007) Real-time estimation of fault rupture extent using near-source versus far-source classification. *Bull Seismol Soc Am* 97(6):1890–1910. <https://doi.org/10.1785/0120060243>
- Yamamoto S, Rydelek P, Horiuchi S, Wu C, Nakamura H (2008) On the estimation of seismic intensity in earthquake early warning systems. *Geophys Res Lett* 35(7):L07302. <https://doi.org/10.1029/2007gl033034>
- Yenier E, Atkinson GM (2015) Regionally adjustable generic ground-motion prediction equation based on equivalent point-source simulations: application to central and Eastern North America. *Bull Seismol Soc Am* 105(4):1989–2009. <https://doi.org/10.1785/0120140332>

Publisher's Note

Springer Nature remains neutral with regard to jurisdictional claims in published maps and institutional affiliations.

Submit your manuscript to a SpringerOpen® journal and benefit from:

- Convenient online submission
- Rigorous peer review
- Open access: articles freely available online
- High visibility within the field
- Retaining the copyright to your article

Submit your next manuscript at ► [springeropen.com](https://www.springeropen.com)